J Wood Sci (2009) 55:241–249
DOI 10.1007/s10086-009-1029-1

REVIEW ARTICLE

Yoshiharu Nishiyama

Structure and properties of the cellulose microfibril

Received: February 4, 2009 / Accepted: March 25, 2009 / Published online: June 10, 2009

Abstract The current structural models of the cellulose microfibril as well as its mechanical and thermal properties are reviewed. The cellulose microfibril can be considered as a single thin and long crystalline entity with highly anisotropic physical properties. The contribution and limit of different methods employed such as electron microscopy, infrared spectroscopy, X-ray scattering and diffraction, solid state nuclear magnetic resonance spectroscopy, and molecular modeling are also discussed.

Key words Cellulose microfibril · X-Ray diffraction · Transmission electron microscopy · ^{13}C solid state NMR · Elastic modulus

Introduction

The fine structure of native cellulose fibers has important implications in the biological processes of plant growth, chemical or enzymatic transformation of cellulosic biomass, and for the conception of new material and understanding of physical properties of a wide range of cellulose-based materials. A considerable part of cellulose research has been devoted to its elucidation. Diverse models and structural concepts have been developed based on different observations and scientific environments, some of them facing counter evidence but still persisting in the literature. Even the term "microfibril" can sometimes generate confusion, because different authors use the term in different ways with closely related terms such as "elementary fibril," "protofibril," or "nanofibers." Although the object under scrutiny has nanometric lateral dimensions, the term "cellulose microfibril" contains notions that are not limited to its size, as will be seen in the following. For this reason this historical term is maintained throughout this review. The common features and variability of the basic component in native cellulose, the microfibril, are outlined with basic observations in support of the model, as well as the limit of the present knowledge.

Y. Nishiyama
CERMAV-CNRS, BP53–38041, Grenoble cedex 9, France
Tel. +33-4-7603-7605; Fax +33-4-7654-7203
e-mail: yoshi@cermav.cnrs.fr

Morphology

The cross section

Oriented native cellulose fiber samples such as ramie give strong X-ray diffraction spots in the direction perpendicular to the fiber axis. The three strongest diffraction spots correspond to spacings of about 3.9, 6.0, and 5.4 Å (Fig. 1), where the 3.9-Å spacing gives the most intense spot. This indicates that the cellulose chains are straight ribbons aligned in the planes, spaced at 3.9 Å. Because all the hydroxyl groups are equatorial to the pyranose ring plane, it is surmised that hydrogen bonding occurs in this plane; this is referred to as the "hydrogen-bonded plane" in the following discussion. Although the approximate molecular conformation and the approximate lateral size of the crystalline region and their orientation have been resolved rather directly by using X-ray diffraction, the organization of the crystallites inside a fibrillar morphology observed with the electron microscope has remained hypothetical for a long time.

In the unicellular giant green alga, *Valonia*, sharp X-ray diffraction patterns can be obtained. The orientation of the crystallographic plane with the 6.0-Å spacing lying parallel to the cell wall was reported by Sponsler.[1] Although this is not the plane where hydrogen bonding is expected, the tendency to orient this plane parallel to the surface has been observed in hydrolyzed wood cellulose,[2,3] and thus a near-rectangular section with the crystallographic surface parallel to the plane with 6.0-Å interplane spacing was conceived as the building block.[4] The interchain distance inside this plane is about 5.4 Å, and is the shortest among different crystallographic planes; it is referred to here as the "dense plane." Based on molecular mechanics calculations, the

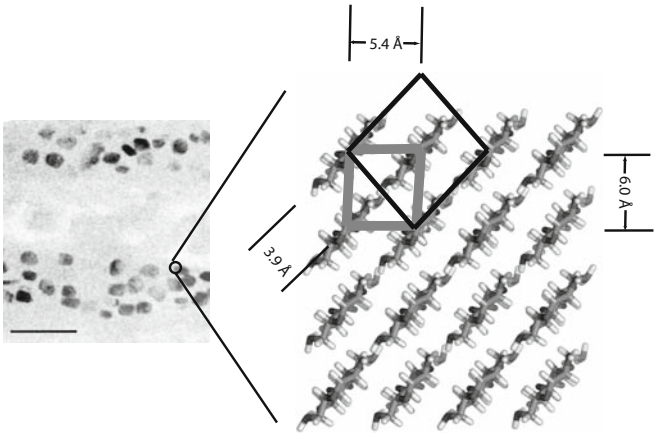

Fig. 1. Bright-field diffraction contrast image of a section of *Valonia ventricosa* (*left*, courtesy of Dr. Chanzy) and a molecular model of cellulose I (*right*) with the monoclinic (*black line*) and triclinic (*thick gray line*) unit cell

formation of this plane was considered to be the most energetically favorable especially in a high-dielectric constant medium[5] such as water, and thus to precede the crystallization event. However, microfibrils having better perfection in the 5.4-Å-spaced "second dense plane," can also be found in different genera in the order of Zygnematales, such as *Spyrogira*,[6] *Micrasterias*,[7]or *Closterium*.[8] In the cell walls of higher plants such as birch[9] or flax,[10] the orientation of the cellulose crystallites is random in a plane perpendicular to the fiber axis.

The imaging of a single crystalline domain by using a diffracted electron beam gave the first direct proof that the crystalline domain extended over the whole width of the microfibril.[11] Furthermore, crystalline lattice has been directly observed for *Valonia*,[12] *Cladophora* microfibrils,[13] and hydrolyzed fragments of ramie fiber,[14] extending over the whole width of the observed microfibril. Lattice images in the cross section of *Valonia* cell wall,[15] oriented microfibrillar bundle in glomerulocytes of tunicate,[16] or acid-hydrolyzed tunicin[17] give directly the cross-sectional shape of the crystals, because the two-dimensional lattice can be obtained only when the chain axis is almost parallel to the electron beam. The *Valonia* cellulose has a square-shaped cross section[18] with the "dense plane" and the "second dense plane" exposed (Fig. 1), whereas tunicate cellulose has a parallelepipedic shape with "dense plane" exposed as the largest facet. The shape also coincided with the earlier diffraction contrast observation and the envelope of microfibril observed by negative staining or heavy metal shadowing. Thus, the microfibrils in these highly crystalline samples essentially correspond to the single crystalline entity.

The concept of microfibrils with a single crystalline core has been further strengthened by considerations of the biosynthesis mechanism. Transmembrane globular structures arranged in two dimensions, called terminal complexes (TCs) have been observed at the fracture surface of the external plasma membrane associated with the impression of microfibrils in different organisms. The arrangement of TCs had close correlation with the morphology of microfibrils produced by the organism, and thus the TCs would simultaneously synthesize many cellulose chains that crystallize into a microfibril. In the case of vascular plants, TCs are considered to have a six-membered rosette morphology on the internal side of the membrane. These rosettes have been observed in a number of organisms associated with cellulose production. In the case of mung bean root, immunogold labeling proved that the rosettes had a high similarity with the cellulose synthase in cotton,[19] and thus the rosette TC is widely accepted as the cellulose synthase complex in higher plants.

Due to the small size and the tendency to tightly associate with each other in the cell wall, the morphology of the microfibrils in higher plants is less clear. The cross-sectional morphology of the microfibril is considered to be close to square or parallelepipedic based on electron micrographs of negatively stained sections of populus tension wood[20] and electron diffraction contrast images of a cross section of flax fiber[10] where square dots can be observed. The lateral dimension of the dots corresponded roughly to the crystallite size estimated from X-ray diffraction line broadening.

The estimation of the cross-sectional dimensions with higher precision is problematic. Atomic force microscopy (AFM) is considered to have high vertical resolution, and thus is potentially capable of precise measurement provided that microfibrils can be sufficiently dispersed on a flat surface. This aspect of AFM seems to be underexploited despite the widespread availability of the technique. Many other techniques have been employed to evaluate microfibril width but most are based on nontrivial assumptions.

Line broadening of X-ray diffraction (XD)

The relation between crystal size and the line broadening of the X-ray diffraction, provided that the broadening due to the instrument is negligible, is straightforward. The peak profile should just follow the Fourier transform of periodic structure with limited size. However, in practice, the measurement of peak width is not obvious, except in a special case where the crystallite size is large enough compared with the unit cell dimensions so that peaks do not overlap. Such cases occur for *Valonia* or tunicin, and the 3.9-Å plane of ramie cellulose, which were the first to be measured by this method.[21]

For other cases, profile analysis based on more or less arbitrary intervention of the experimentalist is required, as was illustrated by Hindeleh and Johnson.[22] They used a third-order polynomial background function and a mixture of Lorentzian and Gaussian functions as the peak function to fit the equatorial intensity profiles. Depending on the mixing ratio of Lorentzian and Gaussian functions, the lateral width of the crystallites varied from 3.35 nm, when integral breadth was taken for 100% Lorentzian peak, to 6.7 nm when peak width at half maximum of a Gaussian peak was taken. The integral breadth should give a weight average of crystallite size provided that the background is

properly subtracted. It should be noted that there is nothing to justify the third-order polynomial or to prefer any other background function. The peak function also depends on the crystal morphology, their size distribution, as well as internal strain and imperfection. Thus, the measure is highly model dependent, and one has to be cautious when comparing the values among different authors.

An important discrepancy exists, even for well-defined thick microfibrils such as those from *Valonia*, between microscopic observation and lateral crystallite size estimated from line broadening. The standard value from microscopic observation is twice as large as the one deduced from X-ray analysis.[23]

Small-angle scattering and negative-staining electron microscopy

Small-angle X-ray scattering (SAXS) was first applied by Heyn[24] to estimate the lateral size of the crystallites in highly oriented fibers. Among different swelling conditions, straight Guinier plots, expected from rod-like morphologies free of interparticle correlations, were obtained for jute swollen in 5% sodium hydroxide or ramie and flax swollen in 1% alkali in the q range of about 0.015–0.1 $Å^{-1}$. The diameter of crystallites, assimilated to cylindrical objects, was estimated from the slope of the plot: for jute, 28 Å; flax, 28 Å; ramie, 43 Å; cotton, 55 Å. The range of diameter corresponded to the results obtained from electron micrographs of sections of the same samples negatively stained using uranyl acetate.[25] However, interpretation of electron micrographs must proceed with caution due to the overlapping of layers,[26] or due to phase-contrast artifacts.[22]

A similar study was performed on *Picea abies* applying SAXS[27] combined with negative-staining transmission electron microscopy (TEM).[28] In this case, the scattering profile was fitted in the range 0.15–0.45 $Å^{-1}$. The minimum of intensity observed at 0.3 $Å^{-1}$ was interpreted as a sign of rather narrow distribution in diameter, in contrast to the wider distribution obtained by TEM ascribed to the grain size of the contrasting agent. However, it has to be noted that the intensity rise after the minimum coincides with the tail of the first diffraction spot at 1 $Å^{-1}$, and thus to interpret the apparent minima as a consequence of homogeneous cross section can be misleading.

Microbeam SAXS of a flax fiber could be fitted by a mean diameter of 19 Å with a standard deviation of 9 Å, or a volume average of 30 Å, in the 0.04–0.4 $Å^{-1}$ range.[29] These values are similar to the 28 Å measured by Heyn, but are significantly smaller than the crystallite width estimated from the line broadening of XD, as mentioned by the authors, even when taking the lowest estimation. Although the homogeneous cylinder model can explain the SAXS feature, a unique solution cannot be derived if the system is polydisperse and departs from the cylindrical morphology. The fact that the estimated diameter was smaller than the smaller limit of crystallite size estimated from XD raises serious doubts on the validity of the method in estimating the microfibril width.

Quantification of surface chain

Other methods are based on the hypothesis that all accessible or amorphous features correspond to the surface chains. The downfield shift of C4 in ^{13}C solid state nuclear magnetic resonance (NMR) spectra at 90 ppm is characteristic of crystalline cellulose, compared with 80 ppm for cellulose in solution. When the crystallinity of cellulose is destroyed by ball milling, the peak occurs at around 85 ppm. A similar situation can be seen for C6 where native cellulose gives a chemical shift of 66 ppm, while ball-milled cellulose has a peak at 63 ppm.[30]

By investigating cellulose from different sources, Earl and VanderHart[31] noticed a correlation between the proportion of surface chain to chain inside the crystal, as estimated from the microscopically determined microfibril size.[31] Wetting the sample resulted in resolution of the higher magnetic field components, which exhibited at least two distinct peaks, as can be seen in the spectra recorded by VanderHart and Atalla.[32] Newman[33] focused on this NMR component, having well-resolved peaks at 84.5 and 83.5 ppm in never-dried kraft pulp, and ascribed it to the surface of the crystallites.

Wickholm et al.[34] obtained the "surface" signal for highly crystalline *Cladophora* cellulose at 84.5 and 83.5 ppm (Fig. 2). Because the latter resonance was more intense, they tentatively assigned the 84.5 and 83.5 ppm signals to the two exposed crystallographic surfaces corresponding to the "second dense plane" and the "dense plane," respectively.[34] In support of this assignment can be found the following observations:

1. A similar difference in intensity is observed on bacterial cellulose (Fig. 2b).[32]

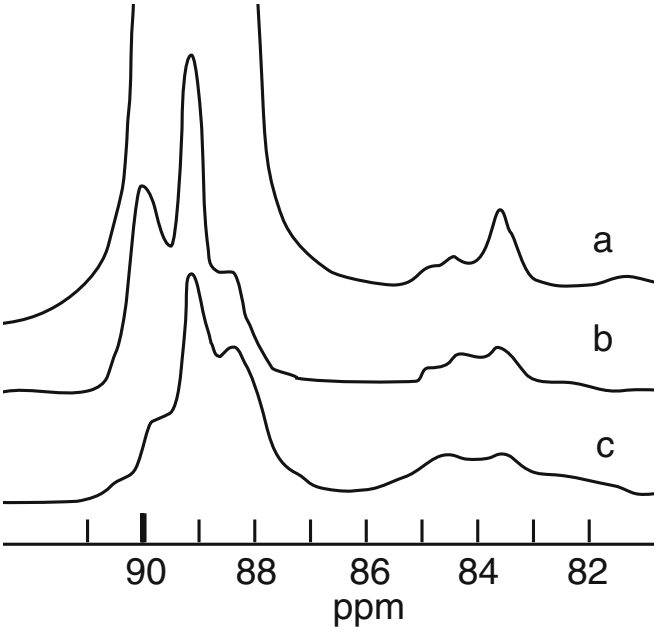

Fig. 2. Solid state ^{13}C nuclear magnetic resonance spectra of C4 region of wet native cellulose. *a*, *Cladophora*;[34] *b*, bacterial;[32] *c*, cotton.[32] Spectra b and c were shifted upfield by 1 ppm to match with more recent spectra

2. The 83.5 ppm component is better defined than the 84.5 ppm component in the tunicate,[34] which does not expose the "second dense plane."[16,17]
3. The peak at 84.5 ppm is more pronounced with samples obtained by glycerol annealing of highly crystalline cellulose III where the "second dense plane" is visibly better developed in the diffraction profile.[35]
4. The longer relaxation time of the 84.5 ppm component (18 s) compared with the 83.5 ppm component (11 s) is also in agreement with molecular dynamics calculation that predicts longer relaxation time for the "dense plane" surface.[36]

The densely packed sheets to behave in a more rigid fashion is also informative. However, further interpretations of the data require various assumptions on the peak profile and would encounter a similar problem to that discussed for XD analysis. Even in "highly crystalline" cellulose, the microfibril cross section displays rounded corners. Thus, a surface constituted purely of two crystallographic planes seems to be an oversimplification.

In the same manner, the state of surface chains can be estimated by the hydrogen–deuterium exchange rate of hydroxyl groups using either infrared spectroscopy[37,38] or neutron inelastic scattering measurements.[39] Both methods give rough agreement with the generally accepted microfibril size, but further ambiguity remains on the evaluation of the depth of the accessible hydroxyl group at a given condition. For infrared investigation, the difference in molar absorption of the OD/OH stretching bands for the crystalline core and surface is another nontrivial parameter.

Longitudinal direction

In highly crystalline cellulose from algae or tunicate, and in bacterial cellulose, it is relatively easy to obtain microfibrils sparsely dispersed to follow individual microfibrils over a long distance. Dark-field or bright-field diffraction contrast images often show patches along the microfibril. It needs to be considered that the diffraction contrast depends on the Bragg condition and thus these images are sensitive to the angle of the crystalline plane with respect to the incident electron beam. These patches often move continuously along the microfibril during the observation probably due to the inclination drift of the supporting membrane. Thus, the microfibril is of single crystalline nature over a long distance along the microfibril, even if twists or strain are also omnipresent.

In higher plants, one of the first microfibrils to be observed in the dispersed state, were those of quince slime, in which glucuronoxylan surrounds the surface preventing the microfibrils from sticking together.[40] This allowed visualization of an individual microfibril over a long distance, sometimes exceeding 6 μm. The majority of the microfibril had a width in the range of 3–5 nm, but some of them were thinner than 2 nm.[41]

Secondary-wall cellulose such as that of wood cellulose needs some chemical treatment to allow good dispersion. Lepoutre and Robertson[42] succeeded in obtaining well-dispersed microfibril of wood pulp by heterogeneous modification of never-dried wood pulp and measured the microfibril width to be in the range of 3.5–4.5 nm. More recently, selective oxidation of primary hydroxyl groups on the surface of microfibrils using never-dried samples,[43,44] or carboxymethylation of never-dried pulp solvent-exchanged in isopropanol[45] were used to facilitate the separation of microfibrils. In all these cases, thin continuous microfibrils with constant lateral size, at least within the resolution of TEM and AFM, of a few nanometers (<5 nm) over a length of a few microns can be seen with occasional kinks. Thus, as a basic rule, microfibrils can be considered as a crystalline entity continuous over a very long distance, having a range of lateral dimension depending on the biological origin and development stage.[46]

Periodic defects along the microfibril have been expected from the acid hydrolysis behavior of cotton fibers. Although "amorphous regions" and "surface chains" on the microfibril share many spectral features,[39] the measurement of chemical reactivity shows the rupture of hydrogen bonding between O3 and the ring oxygen only in this region of defect.[47] Recently, small-angle neutron scattering revealed a Bragg diffraction peak for partially deuterated ramie fiber, indicating a periodical distribution of regions susceptible to deuterium substitution. The weak contrast seen in neutron scattering experiments and the small weight loss during acid hydrolysis indicates that this susceptible part is extremely small compared with the periodicity of 150 nm and represents a few residues every 300 residues.[48]

The origin of the periodical defects along the microfibrils in higher plants is not clear. An interesting observation is reported on cellulose microfibrils produced in vitro from membrane fragments, which cannot be fragmented by acid hydrolysis, whereas the in vivo counterpart will be fragmented as any other cellulose from higher plants.[49] The high density of microfibrils in the cell wall would result in a tight lateral aggregation[3] concentrating the internal strain in a limited zone distributed along the chain axis. The strain accumulates to such a level to induce even the rupture of the O3H-O5 hydrogen bonding.[47]

Crystal structure of cellulose I_α, I_β, and IV_I

As mentioned in the previous section, all native celluloses share a common feature when looking at strong diffraction at low resolution. Small differences had been noticed between bacterial cellulose or *Valonia* cellulose, initially named type A, and higher plant cellulose, named type B, when diffraction spots with smaller intensities or infrared spectra were analyzed.[50] The diffraction from *Valonia* cellulose,[51,52] although very sharp and informative, could only be indexed with a large unit cell comprising eight chains. Solid-state ^{13}C NMR analysis showed that all cellulose spectra could be explained as a linear combination of two subspectra with different combination ratios.[53] Diffraction analysis from a selected area of microfibril containing the pure crystalline form then allowed establishment of two

simple unit cells: a triclinic and one-chain unit cell and a monoclinic two-chain unit cell.[54] Each of them contains two crystallographically independent glucosyl residues. These unit cells imply that the basic difference between the two structures is how the consecutive hydrogen-bonded planes lie on top of each other. If the crystallization is preceded by a lateral association in the dense or second dense plane, the I_α and I_β is determined already at this first event.

Some native celluloses, often giving only blurred diffraction due to the small crystallite size, are assigned to another unit cell called cellulose IV_I similar to I_β but with the monoclinic angle close to a right angle. Due to the peak overlap and broadness, the determination of peak position is quite delicate. Furthermore, the diffraction pattern is the convolution of a Laue function that comes from the lattice repeat, and the molecular form factor inside the lattice. As a consequence, the experimental peak positions are influenced by the slope of the form factor.[55] Cellulose in red meranti has a rectangular unit cell, taking the crystallite size effect into consideration.[56] The cellulose IV_I is very close to cellulose I_β in many features, and the experimental protocol to convert cellulose III to cellulose IV_I generates cellulose I_β of small crystallite size when a highly crystalline sample was employed.[35] However, whether the "real" unit cell in samples classified as cellulose IV_I systematically deviates from the cellulose I_β needs more careful examination.

Parallel-up structure

Although the approximate orientation of the pyranose ring inside the unit cell is rather trivial from the intensity ratios of the three most intense reflections, whether the chains are packed in a parallel or antiparallel manner is less clear. X-Ray fiber crystallography assisted primitive molecular modeling approaches in the 1970s and favored a parallel arrangement.[52,57–59] However, the structures proposed independently by two groups at the time had opposite chain direction inside the unit cell when a common convention was used. French et al.[60] compared different refinement methods and datasets employed by different authors, and concluded that the main limit in discriminating "up" and "down" structure lied in the accuracy of the dataset rather than the computational program utilized. The difference between the "up" and "down" structure is essentially the different relative displacement of the hydrogen-bonded planes. A direct indication for a parallel structure was then obtained by selective staining of the reducing end[61] and directional enzymatic hydrolysis.[62] These methods, however, did not indicate whether the structure was parallel-up or parallel-down. This ambiguity was lifted by combining the reducing end labeling and electron crystallography on a single fragment: the chain polarity could be deduced to be parallel-up according to the standard convention.[63]

The diffraction data could be further improved by using uniaxially oriented specimens composed of relatively large crystallites found in nature. The diffraction data extended to "atomic resolution" of 1 Å with about 300 measurable intensities.[64,65] The direct localization of electron density in reasonable position using a partial model for phasing indicates a high reliability of the method. The parallel-up structure was confirmed in this study.

Hydrogen bonding

Direct evidence of the existence of hydrogen bonding can be readily seen in infrared spectra, which have been published since the 1950s with special emphasis on hydrogen bonding.[50,66] An empirical relation exists between the hydrogen bond distance and the position, width, and intensity of OH stretching bands that shift to lower wavenumber when an acceptor is close.[67] This red shift of the OH stretching band is qualitatively explained as elongation of the OH bond. However, because the cellulose crystal has six independent OH groups in a unit cell, which can couple with each other to give in-phase and out-of-phase bands, the assignment of the spectra can be complex. A general remark can be made that the cellulose I gives stronger parallel bands. This indicates that native cellulose has relatively strong hydrogen bonding along the chain axis and relatively low intermolecular polar interaction. This aspect is quite different from cellulose II and cellulose III, which exhibit OH bands with important red shift perpendicular to the chain direction and small red shift parallel to the chain direction, indicating a more extensive intermolecular hydrogen bonding.

Further insight or resolution can be obtained by external stimulation such as stress or temperature. Hinterstoisser et al.[68–70] used a two-dimensional correlation representation using stress variation on cellulose sheets and discussed on molecular mechanism of load bearing with respect to the hydrogen bonding.[71] However, the measurement was done on only slightly oriented sheets formed by a dynamic former, and thus the stress conditions on each microfibril are far from clear as will be seen in the following section. Highly resolved OH stretching can also be obtained by highly oriented thin films constituted of relatively thick cellulose microcrystals.[72] Maréchal and Chanzy[73] studied highly crystalline cellulose I_β, presenting difference spectra with temperature modulation and the effect of heavy water wetting and drying. It is noted that absorbance builds up at around 3445 cm^{-1} at the expense of the absorption at 3240 cm^{-1}, which disappeared on heating or decreased on drying. This led to the assignment of the most intense and parallel band at 3340 cm^{-1} to the O3H secondary alcohol hydrogen-bonded to the ring oxygen, because it should be quite stable. The band at 3240 cm^{-1} was assigned to a minor population of O2H that strongly hydrogen-bonded to O6 of the subsequent residue. This hydrogen bonding was considered to be easily ruptured by heating or drying.

The location of hydrogen atoms related to hydrogen bonding is difficult to determine by X-ray diffraction techniques: the hydrogen atoms contribute very little to the X-ray scattering, and the hydrogen of the hydroxyl groups are labile. Neutron diffraction has a great advantage in that neutrons interact with hydrogen or deuterium at similar amplitude as carbon and oxygen, and hydrogen and deute-

rium contribute with inverse phase. Thus, deuterium substitution of hydroxyl groups gives a substantial modification in neutron diffraction intensity. The hydrogen position clearly showed up for O3H in the Fourier difference maps using the neutron intensities from deuterated and hydrogenated samples. However, other hydroxyl hydrogens were less clearly localized on the Fourier map, suggesting a hydrogen-bonding disorder.[64,65] The existence of two coexisting hydrogen bonding systems, one major and one minor, was proposed based on structure refinement against neutron data. Both forms of hydrogen bonding lie on the "hydrogen-bonded plane" where the major one corresponds to what was present in most structural models since the scale model.[74] The minor component was refined to a hydrogen bonding having similar feature for Iα and Iβ, but it cannot be excluded that many different hydrogen-bonding schemes exist in reality, as was proposed based on molecular modeling.[75] The structure did not significantly change at low temperature,[76] because the hydrogen bonding did not converge to a single hydrogen-bonding system even at 15 K.[77]

Elastic properties

The linear elastic behavior of a material can be approximated by a second-order tensor, relating the stress tensor and strain tensor. In the system with lowest symmetry, the triclinic system, the number of independent coefficients is 21, whereas in the monoclinic system with $P2_1$ symmetry, the number is 13. However, as will be described in the following, experimental values are sparse, partly due to practical difficulties related to the small crystal size.

The Young's modulus of the crystalline domain has been measured by applying uniaxial tensile load along the fiber axis and monitoring the lattice deformation along the chain axis using X-ray diffraction. This is supposed to correspond to the inverse of a diagonal element of the compliance tensor. Most of the studies have been done on ramie fibers due to its low microfibrillar angle and single fiber length that allows easy manipulation. The stress on each crystallite is in general considered to be identical to the stress applied to the macroscopic sample. The values based on this assumption fall in the range of 115–140 GPa.[78–82] The argument in support of this "series model" (uniform stress) is that the crystalline modulus measured at 9% and 32% moisture content was 130 GPa whereas the macroscopic modulus was 24 and 12 GPa, respectively.[79] However, the uniform stress condition is somewhat contradictory to the current model of the microfibril where long crystalline domains exist along the chain direction with very little, if any, amorphous domain (Fig. 3). If a parallel model is taken, the estimated crystalline modulus would be higher[82] because the cross section of crystal that bears the load will be smaller.

In a series of *Chamaecyparis obtusa* (Hinoki), the ratio of [crystal strain]/[surface strain] was reported to be highly correlated with the microfibrillar angle, and consequently with the tensile modulus along the fiber direction.[83] For wood specimens with small microfibrillar angle, the surface strain was very close to the macroscopic strain. The stress condition would be easier to understand with smaller microfibrillar angle, in which case the deformation clearly follows a parallel situation (uniform deformation). The origin of high macroscopic strain of ramie cellulose compared with crystalline strain remains unclear, although analysis based on combination of parallel and series models can be made.[80,82]

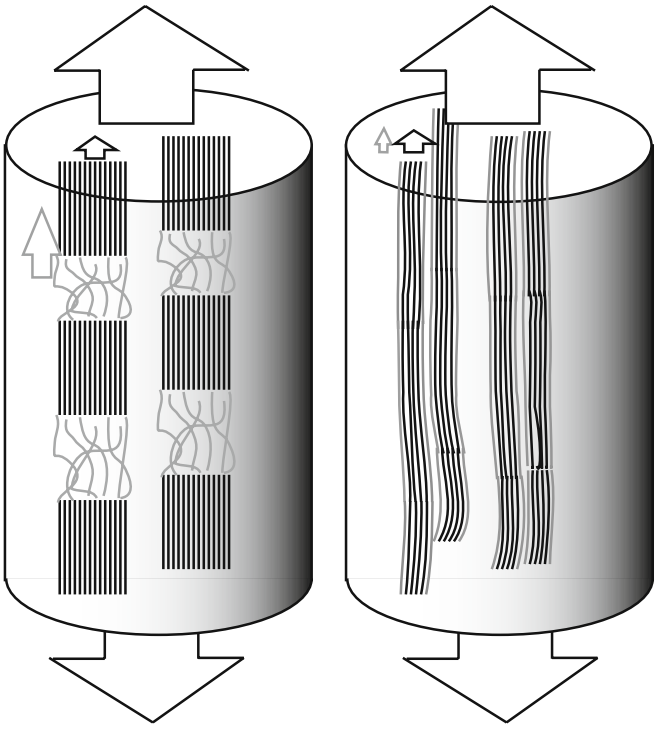

Fig. 3. Series model (*left*) and microfibril model (*right*) of a fiber under tensile stress. The amorphous region or surface chains (*gray lines*) is expected to have lower elastic modulus than the crystalline core (*black lines*). In the series model, all stress is transmitted through crystalline regions, whereas in microfibrils the crystalline core and surface chains share the stress

Another experimental value for tunicate cellulose, 143 GPa,[84] is based on Raman band shift. Strain was applied on two-dimensionally random oriented sample embedded in epoxy resin, where the stress was estimated from the shift of the 1095 cm^{-1} band. The empirical relationship between the band shift with applied stress, common to native and regenerated cellulose[85] was used in this case. The estimation assumes crystal strain to be equal to macroscopic strain and that the efficiency factor that relates Young's modulus of the individual fiber to the modulus of two-dimensional sheet applies at this scale.

The lattice deformation can also be measured in the lateral direction during uniaxial tensile stretching. This is related to the off-diagonal element of the compliance tensor. The strain normal to the hydrogen-bonded plane ε_a can be measured relatively easily because the corresponding diffraction peak is strong and isolated. The ratio $\nu_{ac} = \varepsilon_a/\varepsilon_c$ where ε_c is the strain along the chain direction, does not depend on the assumption of stress condition or mea-

surement of cross-sectional area. The reported values are, however, associated with relatively high estimated errors (standard deviation): 0.56 ± 0.1[86] or 0.38 ± 0.04[87] for ramie and 0.46 ± 0.1[86] for flax.

In the case of wood pulp, a negative apparent v_{ac} was measured after kraft cooking,[88] whereas intact wood specimens always showed positive values.[89] Due to the microfibrillar angle, the internal stress conditions are not sufficiently evident to speculate and needs further understanding of basic properties of the microfibril.

The theoretical elastic modulus can be calculated with small computation resources, provided that the force field and the structure are realistic. Unfortunately, up to now there is no force field able to reproduce the unit cell dimensions of cellulose allomorphs to experimental precision. It is claimed that the mechanical properties can be properly estimated even with a noncomplete force field,[90] however, the calculated elastic properties rely heavily on the starting structure model.[91] Even the contribution of hydrogen bonding to the stiffness varied among studies from 60%[92] to less than 20%.[91] Thus, the quantitative understanding of molecular behavior related to elastic deformation is still a long way away.

A direct measurement of the Young's modulus can also be made by using the relation between sound velocity and density. The X-ray or neutron scattering can probe the density–density correlation in time and space, from which sound velocity in the lattice can be extracted. The signal is dominated by the direction with strong structure factor, and thus the Young's modulus in the direction perpendicular to the hydrogen-bonded plane of 14.8 ± 0.8 GPa was calculated with relatively high precision. In the chain direction, the phonon dispersion could only be measured close to the diffraction position, leading to lower precision, but a value of 220 ± 50 GPa, significantly higher than any other experimental value, is reported.[93]

Thermal behavior

The measurement of anisotropic thermal expansion is more straightforward because it is a first-order tensor, and the temperature is uniform in general. Thermal expansion coefficients have been measured for chain direction on hemlock-spruce and lateral direction on hemp from room temperature to 200°C,[94] lateral direction on cotton,[95] on tunicin[96] and *Cladophora*,[97] and in both directions for tension wood of *Populus maximoviczii*.[98,99] Thermal contraction was observed for chain direction in hemlock-spruce, but the tension wood showed a positive, though small, thermal expansion. The thermal expansion is the greatest in the direction perpendicular to the hydrogen-bonded sheets, of the order of 100 ppm/K when the average is taken between room temperature and 200°C. Between –150°C and room temperature, the value is 70–80 ppm/K for cotton[95] and 46 ppm/K for tunicin.[76] The tension wood showed a negative thermal expansion along the *b*-axis (in the hydrogen-bonded plane) whereas tunicin showed a positive value, suggesting a size effect on the thermal property of microfibrils. The thermal expansion anisotropy is well reproduced in molecular dynamics simulations.[100] The highly anisotropic elastic property and low thermal expansion coefficient along the chain direction result in a low planar thermal expansion when microfibrils form a two-dimensional network.[101]

Acknowledgments The author is indebted to Dr. Henri Chanzy of CERMAV for valuable input to the manuscript and to Dr. Masahisa Wada of the University of Tokyo for critical reading of the manuscript.

References

1. Sponsler OL (1931) Orientation of cellulose space lattice in the cell wall. Additional X-ray data from Valonia cell-wall. Protoplasma 12:241–255
2. Mukherjee SM, Woods HJ (1953) X-Ray and electron microscope studies of the degradation of cellulose by sulphuric acid. Biochim Biophys Acta 10:499–511
3. Elazzouzi-Hafraoui S, Nishiyama Y, Putaux JL, Heux L, Dubreuil F, Rochas C (2008) The shape and size distribution of crystalline nanoparticles prepared by acid hydrolysis of native cellulose. Biomacromolecules 9:57–65
4. Frey-Wyssling A (1955) On the crystal structure of cellulose I. Biochim Biophys Acta 18:166–168
5. Cousins SK, Brown RM Jr (1995) Cellulose I microfibril assembly -computational molecular mechanics energy analysis favours bonding by van der Waals forces as the initial step in crystallization. Polymer 36:3885–3888
6. Kreger AR (1957) New crystallite orientations of cellulose I in *Spirogyra* cell walls. Nature 180:914–915
7. Kim NH, Herth W, Vuong R, Chanzy H (1996) The cellulose system in the cell wall of *Micrasterias*. J Struct Biol 117:195–203
8. Koyama M, Sugiyama J, Itoh T (1997) Systematic survey on crystalline features of algal celluloses. Cellulose 4:147–160
9. Revol JF, Gancet C, Goring DAI (1982) Orientation of cellulose crystallites in the S2 layer of spruce and birch wood cell walls. Wood Sci 14:120–126
10. Näslund P, Vuong R, Chanzy H, Jésior JC (1988) Diffraction contrast transmission electron microscopy on flax fiber ultrathin cross sections. Text Res J 58:414–417
11. Bourret A, Chanzy H, Lazaro R(1972) Crystallite features of *Valonia* cellulose by electron diffraction and dark-field electron microscopy. Biopolymers 11:893–898
12. Sugiyama J, Harada H, Fujiyoshi Y, Uyeda N (1984) High resolution observations of cellulose microfibrils. Mokuzai Gakkaishi 30:98–99
13. Imai T, Putaux JL, Sugiyama J (2003) Geometric phase analysis of lattice images from algal cellulose microbrils. Polymer 44:1871–1879
14. Kuga S, Brown RM Jr (1987) Lattice imaging of ramie cellulose. Polym Commun 28:311–314
15. Sugiyama J, Harada H, Fujiyoshi Y, Uyeda N (1985) Lattice images from ultrathin sections of cellulose microfibrils in the cell wall of *Valonia macrophysa* Kütz. Planta 166:161–168
16. Helbert W, Sugiyama J, Kimura S, Itoh T (1998) High-resolution electron microscopy on ultrathin sections of cellulose microfibrils generated by glomerulocytes in *Polyzoa vesiculiphora*. Protoplasma 203:84–90
17. Helbert W, Nishiyama Y, Okano T, Sugiyama J (1998) Molecular imaging of *Halocynthia papillosa* cellulose. J Struct Biol 124: 42–50
18. Revol JF (1982) On the cross-sectional shape of cellulose crystallites in *Valonia ventricosa*. Carbohydr Polym 2:123–134
19. Kimura S, Laosinchai W, Itoh T, Cui X, Linder CR, Brown RM Jr (1999) Immunogold labeling of rosette terminal cellulose-synthesizing complexes in the vascular plant *Vigna angularis*. Plant Cell 11:2075–2085

20. Goto T, Harada H, Saiki H (1975) Cross-sectional view of microfibrils in gelatinous layer of poplar tension wood (*Populus euramericana*). Mokuzai Gakkaishi 21:537–542
21. Nieduszynski I, Preston RD (1970) Crystallite size in natural celluloses. Nature 225:273–274
22. Hindeleh AM, Johnson DJ (1972) Crystallinity and crystallite size measurement in cellulose fibres: 1. Ramie and fortisan. Polymer 13:423–430
23. Fink HP, Hofmann D, Philipp B (1995) Some aspects of lateral chain order in cellulosics from X-ray scattering. Cellulose 2:51–70
24. Heyn ANJ (1955) Small particle X-ray scattering by fibers, size and shape of microcrystallites. J Appl Phys 26:519–526
25. Heyn ANJ (1966) The microcrystalline structure of cellulose in cell walls of cotton, ramie, and jute fibers as revealed by negative staining of sections. J Cell Biol 29:181–197
26. Preston RD (1974) General principles of wall architecture. In: The physical biology of plant cell walls. Chapman Hall, London pp 163–191
27. Jakob HF, Fratzl P, Tschegg SE (1994) Size and arrangement of elementary cellulose fibrils in wood cells: a small-angle X-ray scattering study of *Piceas abies*. J Struct Biol 113:13–22
28. Jakob HF, Fengel D, Tschegg SE, Fratzl P (1995) The elementary cellulose fibril in *Picea abies*: comparison of transmission electron microscopy, small-angle X-ray scattering, and wide-angle X-ray scattering results. Macromolecules 28:8782–8787
29. Müller M, Czihak C, Vogl G, Fratzl P, Schober H, Riekel C (1998) Direct observation of microfibril arrangement in a single native cellulose fiber by microbeam small-angle X-ray scattering. Macromolecules 31:3953–3957
30. Atalla RH, Gast JC, Sindorf DW, Bartuska VJ, Maciel GE (1980) ^{13}C NMR spectra of cellulose polymorphs. J Am Chem Soc 102:3249–3251
31. Earl WL, VanderHart DL (1981) Observations by high-resolution carbon-13 nuclear magnetic resonance of cellulose I related to morphology and crystal structure. Macromolecules 14: 570–574
32. VanderHart DL, Atalla RH (1984) Studies of microstructure in native celluloses using solid-state ^{13}C NMR. Macromolecules 17: 1465–1472
33. Newman RH (1998) Evidence for assignment of ^{13}C NMR signals to cellulose crystallite surfaces in wood, pulp, and isolated celluloses. Holzforschung 52:157–159
34. Wickholm K, Larsson PT, Iversen T (1998) Assignment of non-crystalline forms in cellulose I by CP/MAS ^{13}C NMR spectroscopy. Carbohydr Res 312:123–129
35. Wada M, Heux L, Sugiyama J (2004) Polymorphism of cellulose I family: reinvestigation of cellulose IV_I. Biomacromolecules 5:1385–1391
36. Bergenstråhle M, Wohlert J, Larsson PT, Mazeau K, Berglund LA (2008) Dynamics of cellulose–water interfaces: NMR spin-lattice relaxation times calculated from atomistic computer simulations. J Phys Chem B 112:2590–2595
37. Horikawa Y, Sugiyama J (2008) Accessibility and size of *Valonia* cellulose microfibril studied by combined deuteration/rehydrogenation and FTIR techniques. Cellulose 15:419–424
38. Horikawa Y, Clair B, Sugiyama J (2009) Varietal difference in cellulose microfibril dimensions observed by infrared spectroscopy. Cellulose 16:1–8
39. Müller M, Czihak C, Schober H, Nishiyama Y, Vogl G (2000) All disordered regions of native cellulose show common low-frequency dynamics. Macromolecules 33:1834–1840
40. Reis D, Vian B, Roland JC (1994) Cellulose-glucuronoxylans and plant cell wall structure. Micron 25:171–187
41. Franke WW, Ermen B (1969) Negative staining of plant slime cellulose: an examination of the elementary fibril concept. Z Naturforsch 24b:918–922
42. Lepoutre P, Robertson AA (1974) Colloidal solutions from sodium polyacrylate-polylacrylamide grafted cellulose. TAPPI 57:87–90
43. Saito T, Nishiyama Y, Putaux JL, Vignon M, Isogai A (2006) Homogeneous suspensions of individualized microfibrils from TEMPO-catalyzed oxidation of native cellulose. Biomacromolecules 7:1687–1691
44. Saito T, Kimura S, Nishiyama Y, Isogai A (2007) Cellulose nanofibers prepared by TEMPO-mediated oxidation of native cellulose. Biomacromolecules 8:2485–2491
45. Wågberg L, Decher G, Norgren M, Lindström T, Ankerfors M, Axnäs K (2008) The build-up of polyelectrolyte multilayers of microfibrillated cellulose and cationic polyelectrolytes. Langmuir 24:784–795
46. Tsuji W, Nakao T, Hirai A, Horii F (1992) Properties and structure of never-dried cotton fibers. III. Cotton fibers from bolls in early stages of growth. J Appl Polym Sci 45:299–307
47. Rowland SP, Roberts EJ (1972) The nature of accessible surfaces in the microstructure of cotton celluloses. J Polym Sci Polym Chem 10:2447–2461
48. Nishiyama Y, Kim UJ, Kim DY, Katsumata KS, May RP, Langan P (2003) Periodic disorder along ramie cellulose microfibrils. Biomacromolecules 4:1013–1017
49. Lai-Kee-Him J, Chanzy H, Müller M, Putaux JL, Imai T, Bulone V (2002) In vitro versus in vivo cellulose microfibrils from plant primary wall synthases: structural differences. J Biol Chem 277:36931–36939
50. Marrinan HJ, Mann J (1956) Infrared spectra of the crystalline modifications of cellulose. J Polym Sci 21:301–311
51. Honjo G, Watanabe M (1958) Examination of cellulose fibre by the low-temperature specimen method of electron diffraction and electron microscopy. Nature 181:326–328
52. Sarko A, Muggli R (1974) Packing analysis of carbohydrates and polysaccharides. III. *Valonia* cellulose and cellulose II. Macromolecules 7:486–494
53. Atalla RH, VanderHart DL (1984) Native cellulose: a composite of two distinct crystalline forms. Science 223:283–285
54. Sugiyama J, Vuong R, Chanzy H (1991) Electron-diffraction study on the two crystalline phases occurring in native cellulose from an algal cell wall. Macromolecules 24:4168–4175
55. Nishimura H, Okano T, Asano I (1981) Fine structure of wood cell walls II. Crystallite size and several peak positions of X-ray diagram of cellulose I. Mokuzai Gakkaishi 27:709–715
56. Nishimura H, Okano T, Asano I (1982) Fine structure of wood cell walls III. On the natural occurrence of cellulose IV. In red meranti. Mokuzai Gakkaishi 28:484–485
57. Gardner KH, Blackwell J (1974) The structure of native cellulose. Biopolymers 13:1975–2001
58. Gardner KH, Blackwell J (1974) The hydrogen bonding in native cellulose. Biochim Biophys Acta 343:232–237
59. Woodcock C, Sarko A (1980) Packing analysis of carbohydrates and polysaccharides. 11. Molecular and crystal structure of native ramie celluloses. Macromolecules 13:1183–1187
60. French AD, Roughead WA, Miller DP (1987) X-Ray diffraction studies of ramie cellulose I. In: Atalla RH (ed) The structures of cellulose. ACS Symposium Series 340. American Chemical Society, pp 15–38
61. Hieta K, Kuga S, Usuda M (1984) Electron staining of reducing ends evidences a parallel-chain structure in *Valonia* cellulose. Biopolymers 23:1807–1810
62. Chanzy H, Henrissat B (1985) Unidirectional degradation of *Valonia* cellulose microcrystals subjected to cellulase action. FEBS Lett 184:285–288
63. Koyama M, Helbert W, Imai T, Sugiyama J, Henrissat B (1997) Parallel-up structure evidences the molecular directionality during biosynthesis of bacterial cellulose. Proc Natl Acad Sci USA 94:9091–9095
64. Nishiyama Y, Langan P, Chanzy H (2002) Crystal structure and hydrogen-bonding system in cellulose I_β from synchrotron X-ray and neutron fiber diffraction. J Am Chem Soc 124:9074–9082
65. Nishiyama Y, Sugiyama J, Chanzy H, Langan P (2003) Crystal structure and hydrogen bonding system in cellulose I_α from synchrotron X-ray and neutron fiber diffraction. J Am Chem Soc 125:14300–14306
66. Marrinan HJ, Mann J (1954) A study by infra-red spectroscopy of hydrogen bonding in celluloses. J Appl Chem 4:204–211
67. Huggins CM, Pimentel GC (1956) Systematics of the infrared spectral properties of hydrogen bonding systems: frequency shift, half width and intensity. J Phys Chem 60:1615–1619
68. Hinterstoisser B, Salmén L (1999) Two-dimensional step-scan FTIR: a tool to unravel the OH-valency-range of the spectrum of cellulose I. Cellulose 6:251–263

69. Hinterstoisser B, Salmén L (2000) Application of dynamic 2D FTIR to celluloses. Vib Spectrosc 22:111–118
70. Hinterstoisser B, Åkerholm M, Salmén L (2001) Effect of fiber orientation in dynamic FTIR study on native cellulose. Carbohydr Res 334:27–37
71. Hinterstoisser B, Åkerholm M, Salmén L (2003) Load distribution in native celluloses. Biomacromolecules 4:1232–1237
72. Nishiyama Y, Isogai A, Okano T, Müller M, Chanzy H (1999) Intracrystalline deuteration of native celluloses. Macromolecules 32:2078–2081
73. Maréchal Y, Chanzy H (2000) The hydrogen bond network in Iβ cellulose as observed by infrared spectrometry. J Mol Struct 523:183–196
74. Jones DW (1958) Crystalline modifications of cellulose. Part III. The derivation and preliminary study of possible crystal structures. J Polym Sci 32:371–394
75. Mazeau K (2005) Structural micro-heterogeneities of crystalline Iβ-cellulose. Cellulose 12:339–349
76. Langan P, Sukumar N, Nishiyama Y, Chanzy H (2005) Synchrotron X-ray structures of cellulose Iβ and regenerated cellulose II at ambient temperature and 100 K. Cellulose 12: 551–562
77. Nishiyama Y, Johnson GP, French AD, Forsyth VT, Langan P (2008) Neutron crystallography, molecular dynamics, and quantum mechanics studies of the nature of hydrogen bonding in cellulose Iβ. Biomacromolecules 9:3133–3140
78. Sakurada I, Nukushina Y, Itoh T (1962) Experimental determination of the elastic modulus of crystalline regions in oriented polymers. J Polym Sci 57:651–660
79. Sakurada I, Ito T, Nakamae K (1966) Elastic moduli of the crystal lattices of polymers. J Polym Sci C 15:75–91
80. Matsuo M, Sawatari C, Iwai Y, Ozaki F (1990) Effect of orientation distribution and crystallinity on the measurement by X-ray diffraction of the crystal lattice moduli of cellulose I and II. Macromolecules 23:3266–3275
81. Nishino T, Takano K, Nakamae K (1995) Elastic modulus of the crystalline regions of cellulose polymorphs. J Polym Sci Polym Phys 33:1647–1651
82. Ishikawa A, Okano T, Sugiyama J (1997) Fine structure and tensile properties of ramie fibres in the crystalline form of cellulose I, II, III_I and IV_I. Polymer 38:463–468
83. Nakai T, Yamamoto H, Nakao T, Hamatake M (2006) Mechanical behavior of the crystal lattice of natural cellulose in wood under repeated uniaxial tension stress in the fiber direction. Wood Sci Technol 40:683–695
84. Šturcová A, Davies GR, Eichhorn SJ (2005) Elastic modulus and stress-transfer properties of tunicate cellulose whiskers. Biomacromolecules 6:1055–1061
85. Eichhorn SJ, Hughes M, Snell R, Mott L (2000) Strain induced shifts in the Raman spectra of natural cellulose fibers. J Mater Sci Lett 19:721–723
86. Kölln K (2004) Morphologie und mechanische Eigenschaften von Zellulosefasern: Untersuchungenmit Röntgen-und Neutronenstreuung. PhD thesis Christian-Albrechts-Universität zu Kiel
87. Nakamura K, Wada M, Kuga S, Okano T (2004) Poisson's ratio of cellulose Iβ and cellulose II. J Polym Sci Polym Phys 42: 1206–1211
88. Peura M, Grotkopp I, Lemke H, Vikkula A, Laine J, Müller M, Serimaa R (2006) Negative Poisson ratio of crystalline cellulose in kraft cooked Norway spruce. Biomacromolecules 7:1521–1528
89. Peura M, Kölln K, Grotkopp I, Saranpää P, Müller M, Serimaa R (2007) The effect of axial strain on crystalline cellulose in Norway spruce. Wood Sci Technol 41:565–583
90. Tanaka F, Iwata T (2006) Estimation of the elastic modulus of cellulose crystal by molecular mechanics simulation. Cellulose 13:509–517
91. Eichhorn SJ, Davies GR (2006) Modelling the crystalline deformation of native and regenerated cellulose. Cellulose 13:291–307
92. Tashiro K, Kobayashi M (1991) Theoretical evaluation of three-dimensional elastic constants of native and regenerated celluloses: role of hydrogen bonds. Polymer 32:1516–1526
93. Diddens I, Murphy B, Krisch M, Müller M (2008) Anisotropic elastic properties of cellulose measured using inelastic X-ray scattering. Macromolecules 41:9755–9759
94. Takahashi M, Takenaka H (1982) X-Ray study of thermal expansion and transition of crystalline celluloses. Polym J 14:675–679
95. Seitsonen S, Mikkonen I (1973) X-Ray study on the thermal expansion of cotton cellulose. Polym J 5:263–267
96. Wada M, Kondo T, Okano T (2003) Thermally induced crystal transformation from cellulose Iα to Iβ. Polym J 35:155–159
97. Wada M (2002) Lateral thermal expansion of cellulose Iβ and III_I polymorphs. J Polym Sci Polym Phys 40:1095–1102
98. Kim DY, Nishiyama Y, Wada M, Kuga S, Okano T (2001) Thermal decomposition of cellulose crystallites in wood. Holzforschung 55:521–524
99. Hori R, Wada M (2005) The thermal expansion of wood cellulose crystals. Cellulose 12:479–484
100. Bergenstråhle M, Berglund LA, Mazeau K (2007) Thermal response in crystalline Iβ cellulose: a molecular dynamics study. J Phys Chem B 111:9138–9145
101. Nogi M, Ifuku S, Abe K, Handa K, Nakagaito AN, Yano H (2006) Fiber-content dependency of the optical transparency and thermal expansion of bacterial nanofiber reinforced composites. Appl Phys Lett 88:133124–133124.3